sciendo
ISSN 1335-8871
MEASUREMENT SCIENCE REVIEW
Journal homepage: https://content.sciendo.com

Estimation of Blood Calcium and Potassium Values from ECG Records

Sebahattin Babur[1*], Sanam Moghaddamnia[2], Mehmet Recep Bozkurt[1]

[1] *Sakarya University, Electrical and Electronics Engineering, 54050, Sakarya, Turkey,*
sebahattin.babur3@ogr.sakarya.edu.tr, mbozkurt@sakarya.edu.tr
[2] *Turkish-German University, Electrical and Electronics Engineering, 34820, İstanbul, Turkey, moghaddamnia@tau.edu.tr*

Abstract: The identification of diseases caused by changes in ion concentration is quite difficult and yet plays a decisive role in the success of clinical care, diagnosis and treatment. The clinically proven approach to diagnosing electrolyte concentration imbalance is blood tests. There is a need to provide a non-invasive diagnostic method that is not of a temporary nature. Bio-signals such as the electrocardiogram (ECG) can be used to meet this demand and become diagnostic tools that facilitate home monitoring of electrolyte concentration on a permanent basis. This study investigates the feasibility and efficiency of methods based on machine learning (ML) and ECG recordings in monitoring critical levels of existing potassium and calcium concentration. Morphological, frequency and frequency-time domain features were extracted to automatically estimate calcium and potassium levels. Furthermore, the potential of estimates based on modeling approaches will be demonstrated to gain insights into relevant clinical findings and improve the performance of monitoring approaches. Using the hold-out validation method, the best results in terms of mean square error (*MSE*) and *R* for estimating the calcium value are 0.7157 and 0.57347, using fuzzy inference systems (FIS). Here, *R* represents the proportion of the variance in the calcium value that is explained by the model.

Keywords: Bio-signals, chronic kidney disease, ion concentration, machine learning, non-invasive diagnostic.

1. INTRODUCTION

This research addresses the challenge of diagnosing diseases associated with ion concentration changes by proposing a non-invasive diagnostic method that goes beyond temporary measures. Unlike traditional blood tests, which are clinically accepted but invasive, this study explores the use of electrocardiogram (ECG) or bio-signal for continuous home monitoring of electrolyte concentration. Chronic kidney disease (CKD) is one of the most common diseases, affecting about 13.1 % of the population in the United States and about 18.38 % in Europe [1], [2]. As a result of kidney failure, there are changes in the blood serum electrolyte concentrations of patients. Calcium, potassium and sodium are among the electrolytes that affect the electrophysiology of the heart. Patients with CKD therefore have a high risk of cardiovascular disease [3]. Hyperkalemia and hypokalemia in potassium are common causes of sudden cardiac deaths in clinical trials. To prevent such fatal outcomes, potassium (K+) disorders must be promptly detected and treated [4], [5].

Currently, dyskalemia is diagnosed by laboratory tests. Bedside blood tests provide a temporary analysis of electrolyte levels. However, the accuracy and precision of these tests may not be as reliable as that of a central clinical laboratory. Bedside point-of-care tests performed by nurses in emergency departments showed a high correlation with central laboratory results for several analytes, with only 3 out of 400 measurements exceeding clinically acceptable deviations [6]. The main reason for this discrepancy is that the estimated plasma K+ concentration falls short of the actual value, making it difficult to differentiate from hemolysis pseudohyperkalemia [7], [8]. Electrocardiography (ECG) is an essential test for cardiac and non-cardiac emergency patients, whose condition may show typical changes that occur in dyskalemia, as heart tissue is highly susceptible to this condition. Major ECG changes associated with hypokalemia include decreased T-wave amplitude, ST-segment changes, T-wave reversal, prolonged PR interval, and prolonged QT interval (QTc) [9]. Typical ECG findings for hyperkalemia range from long crested T waves and a shortened QT interval to a prolonged PT interval and the disappearance of the P wave. Followed by a widening of the QRS complex, and finally a sinus wave morphology [9], [10]. Although these morphological changes are well known in dyskalemia, even experienced clinicians often struggle to recognize all these signs [11].

DOI: 10.2478/msr-2024-0022
Corresponding author: sebahattin.babur3@ogr.sakarya.edu.tr, (Sebahattin Babur)

The main contribution of this study is the proposal of a reliable regression approach for detecting anomalies in calcium and potassium levels using feature extraction in the time- and frequency-domain and machine learning (ML). The study focuses on supervised ML and considers the analysis of temporal morphological features and frequency variations based on ECG recordings used as input. Many studies have shown the potential of morphological features for potassium and calcium detection. However, there is no study on the relationship between ion concentrations and features in the time and frequency domain.

The choice of multilayer feed-forward artificial neural networks (ANNs) and fuzzy inference systems (FIS) is based on their different and complementary advantages. ANNs have the potential to capture complicated and non-linear correlations, which makes them highly flexible and powerful. On the other hand, FIS excel in providing interpretability and effective handling of uncertainty. Other methods, while potentially useful, generally lack the necessary adaptability, interpretability or ability to simulate non-linear interactions as successfully as the selected methods. Thus, ANNs and FIS offer a well-balanced method that combines accurate predictions with the ability to analyze results and incorporate expert knowledge.

The rest of this article is organized as follows: Section 2 provides an overview of the current state of research in this area. Section 3 provides relevant information about the database used. Section 4 provides a brief introduction to the analysis of morphological, frequency and time-frequency domain-based ion concentrations, followed by a detailed description of the applied ML methods. In Section 5, the evaluation results of the proposed system are presented and discussed. Finally, we conclude the article by highlighting the main contributions and providing future research directions.

2. BACKGROUND & RELATED WORK

Potassium is the most important intracellular electrolyte. In the organism, it is largely an intracellular cation that influences blood levels and neuromuscular activity in general. Many signs and symptoms of excess potassium (hyperkalemia) occur in the cardiovascular, central nervous and muscular systems. The potassium balance is regulated in the kidneys. Therefore, the urine contains most of the potassium lost from the organism [12], [13].

In patients with end-stage renal failure, a series of hydro-electrolytic changes occur due to the lack of internal environment regulation, which is a fundamental function of the kidneys. Of these changes, hyperkalemia often affects neuromuscular symptoms, electrocardiographic changes and cardiac arrhythmias [14], [15]. As hyperkalemia worsens, potentially fatal electrocardiographic changes occur, manifested by high T waves, a prolonged P-R interval, bradycardia, ventricular arrhythmias, and flattening or absence of the P wave [16].

Determination of the serum level of this electrolyte in the laboratory may take some time. Electrocardiographic monitoring [9] and simultaneous documentation of the patient's symptoms can be very helpful when results are published. An ECG can be a very useful diagnostic tool if a specialist is aware of the changes that can occur in abnormal situations [14].

In addition, this diagnostic tool can help to quickly determine whether renal functions in hemodialysis patients are due to various causes such as weakness, muscle weakness and fatigue [17], [18]. Similarly, several articles [9], [17]-[19] concluded that patients with CKD tolerate hypercalcemia better in their final stages and have fewer arrhythmias and neuromuscular manifestations than people with normal kidney function.

Corsi et al. found that potassium concentration in the blood has an influence on the ECG and in particular on the T wave. 69 samples (3 separate measurements from 23 hemodialysis patients) comprise the developed ECG-based potassium estimator. The authors developed an estimation scheme based on the ratio between the decreasing slope of the T-wave in the ECG signal and the amplitude value of the T-wave and tested it on 12 samples. According to the test results, the absolute error and standard deviation amount to 0.43 ± 0.28 mM, respectively. This study has shown that the proposed method is effective for monitoring patients at risk of hyper- and hypokalemia [20].

Corsi, DeBie et al. analyzed 12-lead ECGs from 45 hemodialysis patients and 12 patients with Long QT Syndrome (LQT) for the non-invasive measurement of blood potassium concentration from ECGs of hemodialysis patients. They determined the amplitude and the decreasing slope of the T-wave as relevant attributes. The quality of the presented estimation was evaluated by cross-validation. It was shown that there is a relationship between the K-ECG (potassium ECG) and the references [K+] from blood samples. According to the results of the test dataset, the absolute error and standard deviation are -0.09 ± 0.59 mM and 0.46 ± 0.39 mM, respectively. The method proposed in the study has been shown to be effective in monitoring patients at risk of hyper- and hypokalemia [21].

Mesa, Pilia et al. investigated the efficiency of derivative reduction methods in estimating serum calcium and potassium concentration levels. The estimator was developed using the standard derivative of ECG signals. The electrical signals converted from the heart were obtained as a result of lead V2 reduction of the concentrations in the blood by lead reduction methods. They calculated five features describing the electrolyte changes from the signals by using principal component analysis (PCA) and maximum amplitude conversion. They used a first- and third-order polynomial equation combining the calculated features and concentration values to reconstruct the ion concentrations. In addition, 30 dB of white Gaussian noise was added to the ECGs to simulate clinically measured signals.

The analysis results showed that the estimate of potassium and calcium obtained by first-order polynomial regression was 0.0003 ± 0.0767 mmol/l (mean ± standard deviation) and -0.0036 ± 0.1710 mmol/l, respectively. For the noisy signal scenario, the obtained results are -0.003 ± 0.2040 and -0.0002 ± 0.2040 mmol/l for potassium and calcium, respectively [22].

Sánchez et al. found that potassium-related electrocardiographic changes were assessed in patients with end-stage CKD and compared with previous studies. The study measured the pre- and post-dialysis serum potassium and other electrolyte concentrations of hemodialysis patients, and obtained simultaneous 12-lead ECG signals in the first session. All ECGs of the patients were analyzed by a specialist physician, and 39 patients with a mean age of 67.35 (24-89) were included in the study, of whom 58.9 % were female and 41.1 % were male. The range of serum potassium before hemodialysis was between 2.8 and 7.4 mEq/l (mean 5.07 mEq/l). Thus, 29.4 % of patients had serum potassium levels of 5.5 mEq/l, with the peak value of T waves in leads V2 showing the most frequent change. In addition, the mean height of the T-wave in hyperkalemia in leads V4 was 7 mm. The results show that ECG can be a useful tool for early prediction and diagnosis of hyperkalemia [23].

Mesa, Pilia et al. studied the effects of electrolyte fluctuation on cardiac signals (action potential and ECG) using an estimation model to investigate the link between CKD and cardiovascular disease. The first step was to look at the ventricular cell model at the cellular level, taking into account different levels of sodium (Na+), calcium (Ca2+) and potassium (K+) outside the cells, which are similar to those seen in people with CKD. They calculated a 12-lead ECG using the simulations proposed in the article. The results at the cellular and ventricular levels are consistent with the literature. In addition, new features to represent electrolyte changes were proposed in [23], which may be useful for further studies to estimate ion concentrations based on ECG recordings [24].

Pilia and Dössel proposed a method for reconstructing the calcium and potassium ion concentration from the ECG. In a first step, 91 monodomain simulations were performed with ten Tusscher ventricular cell models for different extracellular ion concentrations. This study resulted in a standard 12-lead ECG. ECGs with changes in calcium and potassium levels, amplitude and morphological differences were obtained. In the second step, simulated ECG signals were used to reconstruct ion concentrations directly from the ECG recordings. They used the features extracted from the signals to determine the changes caused by different ion concentrations. An artificial neural network (NN) solves the inverse problem, which involves recovering the ECG properties from the ion concentrations. Potassium estimation results were calculated using seven-fold cross-validation and an error value of 0.00 ± 0.28 mmol/l (mean ± standard deviation) was obtained. The estimation error for calcium was 0.00 ± 0.08 mmol/l [25].

Using supervised ML, Dillon et al. presented 12 repolarization-related features selected for ion concentration detection. Moreover, in this study, normal and abnormal situations and the values of ion concentration are determined by supervised ML algorithms based on the features derived from the frequency changes of ECG signals. In our study, we try to increase the success by combining morphological features with frequency and time-frequency domain-based techniques and supervised ML algorithms [26].

3. DATABASE

Beth Israel Deaconess Medical Center in Boston, Massachusetts, registered the MIMIC III database between 2001 and 2012. We used the latest version (v1.4) for this study. The MIMIC III database contains 58,976 referrals of 46,520 patients. The criteria shown in Fig. 1 and Fig. 2 were applied to filter out patients who had a sufficient minimum amount of data for analysis. Table 1 shows the characteristics of the final data set.

Table 1. Classification of feature groups.

Feature	Number
Time domain	24
Morphological features	12
ICD codes	1
Demographics (age)	1
Frequency domain	3
Time-frequency domain	20
Total	61

A subset of waveform records contains sufficient information to reliably identify the patient records, and these records match the time period represented by the MIMIC III Clinical Database [27]. We use all available information, either through manual corrections or mainly through automated matching processes. We can match a total of 22,317 waveform records (34 %) in the database to a corresponding patient in the clinic.

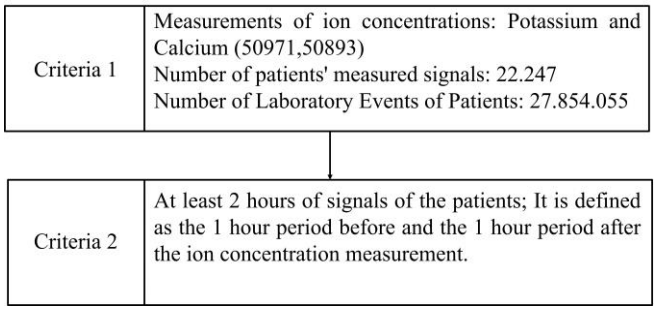

Fig. 1. Exploring ion concentrations in patient data in the MIMIC III database.

All data associated with a particular patient is stored in a single subdirectory named after the patient's MIMIC III ID. Ten intermediate levels (match/p00 to match/p09) further subdivide these subdirectories.

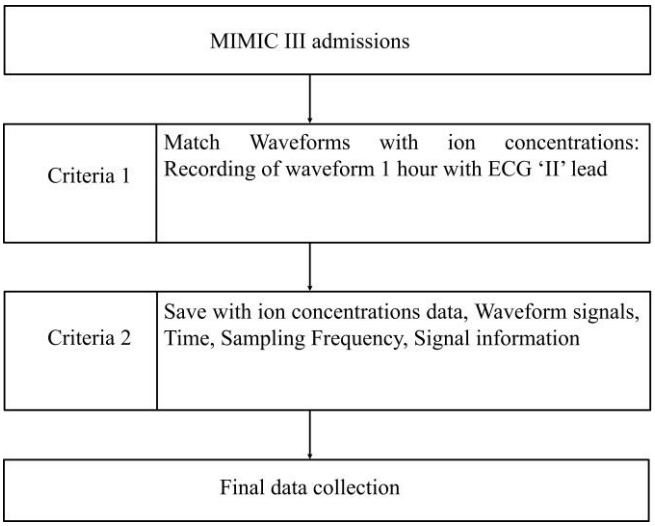

Fig. 2. MIMIC III Admissions data processing flow.

The name of each matched waveform record has the format Matched /pXX /pXXNNNN /pXXNNNN-YYYY-MM-DD-hh-mm; where XXNNNN is the matched MIMIC III Clinical Database SubjectID and YYYY, MM, DD, hh, and mm, year, month (01-12), day (01-31), actual hour (00-23), and minutes (00-59), which are derived from the start date and time. These data match the corresponding data records in the MIMIC III Clinical Database.

This flowchart, shown in Fig. 3, outlines the basic steps in developing a predictive model for determining blood calcium and potassium levels. The flowchart consists of five main steps:

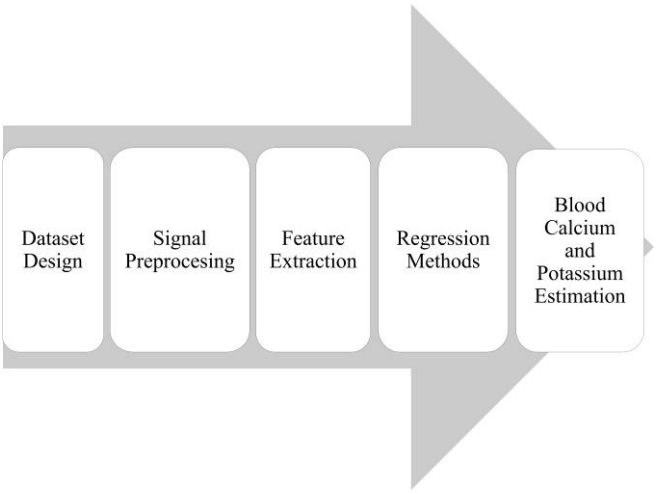

Fig. 3. Processing approach block diagram.

- 'Dataset Design' refers to the process of carefully selecting and structuring the data to be used to train the model. In this step, we select the data collection methods and decide which data to use.
- 'Signal Pre-processing' involves the preparation of the raw ECG signals to prepare them for use in the model. This process may include the implementation of noise reduction, signal filtering and signal normalization techniques.
- 'Feature Extraction': The process of extracting relevant features from processed signals to train the prediction model is called 'Feature Extraction'. These features represent unique data derived from the signals.
- 'Regression Methods': Using a range of statistical and ML methods with the extracted features to predict calcium and potassium levels. In this step, experiments are performed with several regression models and then the one with the best performance is selected.
- 'Blood Calcium and Potassium Estimation' refers to the evaluation of whether the model accurately predicts the amounts of calcium and potassium in the blood samples, which is the final outcome of the process. This step is crucial as it determines the accuracy and reliability of the model.

The arrows in the flowchart illustrate the transition from one process to another and highlight the interdependence of each phase, paving the way for the subsequent phase. This illustrated that the effectiveness of the predictive model depends on the excellence and thoroughness of the tasks performed in each step. The modeling process requires a methodical and comprehensive strategy to extract meaningful information from complicated biological signals.

4. METHODS

In this section, we will thoroughly examine the core components of the predictive model and the methods used. First, we discuss the signal pre-processing and feature extraction processes, followed by an explanation of how ML and FIS are integrated to improve prediction accuracy. Each of these steps is crucial in influencing the model's performance, and in the following subsections we will focus on a detailed analysis of these processes.

A. Binary feature labeling from MIMIC III

The MIMIC III dataset assigns International Classification of Diseases (ICD) codes to patient records. In particular, Table 2 lists the relevant ICD codes for renal disease. This approach allows researchers to effectively identify and analyze patients with kidney-related conditions.

Table 2. ICD codes for kidney diseases' stages.

ICD code	Description
5851	CKD, Stage I
5852	CKD, Stage II
5853	CKD, Stage III
5854	CKD, Stage IV
5855	CKD, Stage V
5859	CKD, Unspecified

Age is another feature that we had to group. The MIMIC III dataset posed a challenge for age analysis, as the age value for patients over 89 years falls in the range of 300. To address this issue, we classified age into 20-year bins, as shown in Table 3. This allowed us to treat patients whose age was reported as 300 without having to exclude them from our analysis.

Table 3. Categorizing age group.

Group age range	Description
< 20	1
21 - 40	2
41 - 60	3
> 61	4

B. Signal pre-processing

ECG recordings are often affected by various types of artifacts and noise, including baseline wander, muscle artifacts, electrical interference and motion artifacts, which limit the usability of the ECG signals and have to be removed. In the first step of pre-processing, baseline shift/wander correction is performed. A band-pass filter (5 Hz-100 Hz) is then used for denoising. In the last step, we perform a predictive isolation correction to obtain clean ECG signals.

The ECG is a standard, cost-effective, and non-invasive tool for the early detection of various heart diseases. It can provide important information about underlying cardiac function by depicting the strength, timing and morphology of electrical signals propagating through the heart.

The extracted features require the identification of the peak of each ECG waveform (P-wave, QRS complex, T-wave) as well as their open and offset-determining reference points. For this purpose, the filter bank method is used, which essentially utilizes the continuous wavelet transform. The flow diagram of the applied algorithm is shown in Fig. 4.

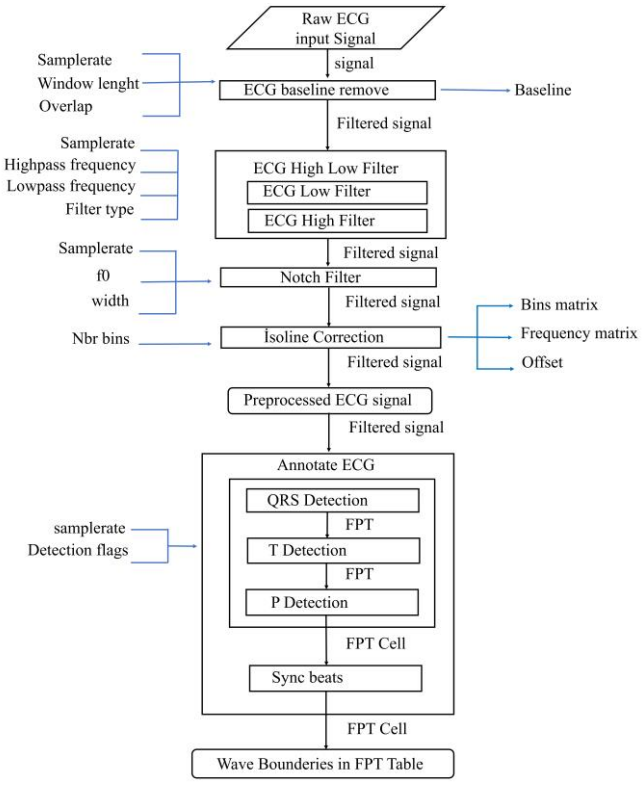

Fig. 4. Pre-signal processing P, QRS, T detection proposed algorithm [28].

Fig. 5 illustrates the different stages of pre-processing raw ECG signals to prepare them for further analysis. The pre-processing stages are crucial to ensure that the data used for modeling is clean and reliable.

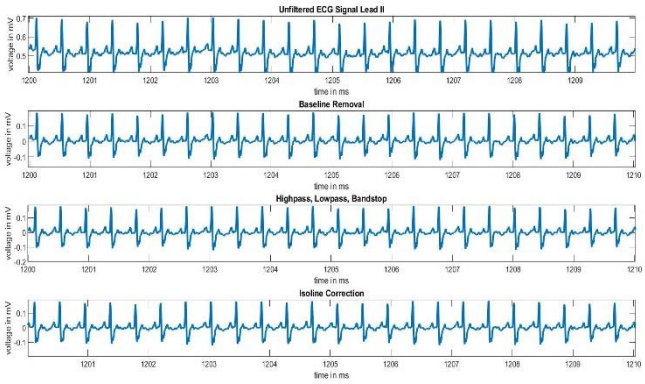

Fig. 5. Signal pre-processing stages a) Raw ECG signal b) Baseline removed c) High and low pass filtering d) Clean signal.

Fig. 6 shows the results of applying the FilterBank method to the ECG signal and highlights the detected P, QRS and T points. The accurate detection of these points is crucial for analyzing the electrical activity of the heart and for extracting features used for the predictive model.

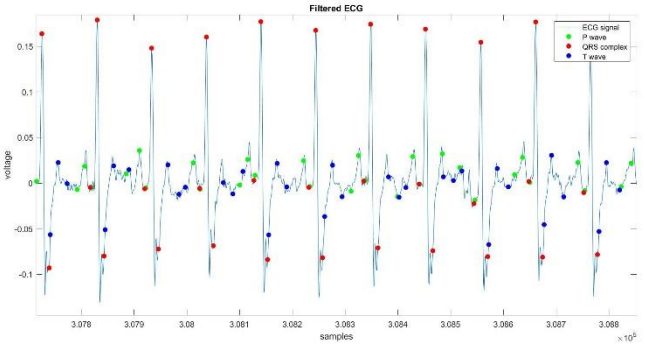

Fig. 6. Detection of P-QRS-T points with the FilterBank method.

C. Feature extraction

In general, feature extraction is the first step in most signal processing applications. In general, we perform feature extraction in the time, frequency and time-frequency domains. Morphological feature extraction requires splitting the biomedical signal into short frames to obtain local information. We then extract a feature vector for each frame. Features in the frequency domain are also extracted. Both time and frequency domain features have been successfully used for classification purposes in previous studies [29]-[30].

1) Time domain and morphological features

We extracted 12 ECG features for in-depth analysis based on initial data and physiological significance. These features include the amplitude of P-, R- and T-waves, PR and QT intervals, PR and ST segments, QRS complex, R-T duration, right slope (T right slope), left slope (T left slope) and the ratio of the T-wave amplitude to the T right slope. We have

developed automatic algorithms to extract these 12 features. Fig. 7 illustrates the extraction process and representation of these features.

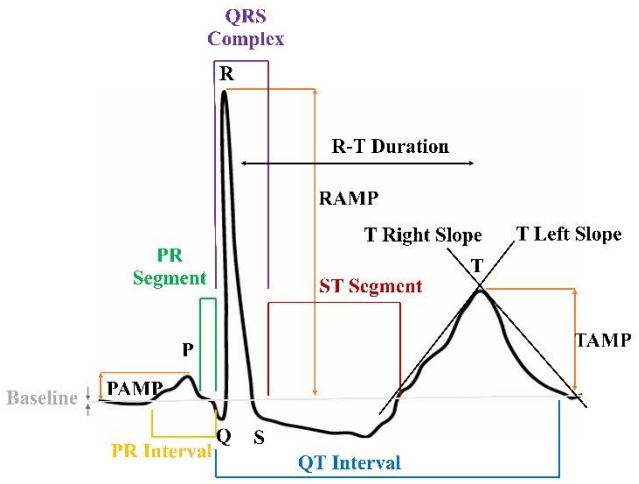

Fig. 7. ECG morphological features evaluated to determine concentrations changes [26].

Basic metrics such as mean, standard deviation and root mean square (RMS) are examples of statistical features. This feature set also includes statistics for skewness, form factor and higher-order kurtosis. These statistical measurements can detect deviations from typical signal behavior and are sensitive to changes in the signal patterns, especially when failing fault signs are present.

➢ *Shape factor*

RMS divided by the mean of the absolute value yields this value. The signal's shape affects the shape factor (SF), which is unaffected by the signal's dimensions.

$$x_{SF} = \frac{x_{rms}}{\frac{1}{N}\sum_{i=1}^{N}|x_i|} \tag{1}$$

The higher-order statistics provide valuable insight into the behavior of a system by examining the kurtosis (fourth moment) and skewness (third moment) of the signal.

➢ *Kurtosis*

Kurtosis refers to the extent of the tails of a signal distribution and indicates the susceptibility of the signal to outliers. The occurrence of anomalies during development can lead to a higher number of outliers, resulting in an increased value of the kurtosis metric.

$$x_{Kurtosis} = \frac{\frac{1}{N}\sum_{i=1}^{N}(x_i-\bar{x})^4}{\left[\frac{1}{N}\sum_{i=1}^{N}(x_i-\bar{x})^2\right]^2} \tag{2}$$

➢ *Skewness*

The presence of asymmetry in the distribution of a signal. Changes can affect the evenness of the distribution and thus increase the degree of asymmetry.

$$x_{Skewness} = \frac{\frac{1}{N}\sum_{i=1}^{N}(x_i-\bar{x})^3}{\left[\frac{1}{N}\sum_{i=1}^{N}(x_i-\bar{x})^2\right]^{3/2}} \tag{3}$$

Impulsive metrics refer to the features associated with the highest points of the signal.

➢ *Peak value*

Peak value is the highest absolute value of a signal. Used to calculate the remaining impulse metrics.

$$x_{Peak} = \max_i |x_i| \tag{4}$$

➢ *Impulse factor*

Impulse factor determines the ratio between the peak height and the average level of the signal.

$$x_{Impulse} = \frac{x_{Peak}}{\frac{1}{N}\sum_{i=1}^{N}|x_i|} \tag{5}$$

➢ *Crest factor*

We calculate the crest factor by dividing the peak value by the RMS value. Typically, changes in the signal's peakiness reveal problems before they manifest themselves in the signal's root mean square energy. The crest factor can serve as an initial indicator of problems in the early stages of their development.

$$x_{Crest} = \frac{x_{Peak}}{\sqrt{\frac{1}{N}\sum_{i=1}^{N}x_i^2}} \tag{6}$$

➢ *Clearance factor*

We calculate the clearance factor by dividing the peak value by the squared mean value of the square roots of the absolute amplitudes.

$$x_{Clearance} = \frac{x_{Peak}}{\left(\sqrt{\frac{1}{N}\sum_{i=1}^{N}\sqrt{|x_i|}}\right)^2} \tag{7}$$

➢ *Signal quality metrics*

The signal processing metrics include functions for measuring distortions. System degradation can lead to an increase in noise level, a change in the harmonic ratio to the fundamental frequency or both simultaneously.

- The signal-to-noise ratio (SNR) is defined as the ratio of the power of the signal to the power of the noise.
- The signal-to-modulation-to-noise ratio (SMNR) is a measure that quantifies the degree of random variation compared to the pure periodicity [37]. It can be calculated using the following estimates:

$$S = \sum_{k=1}^{K} p_x(k) \tag{8}$$

where $p_x(k)$ is the SMNR at the frequency component k.

- The total harmonic distortion (THD) is defined as the ratio of the power of all harmonic components to the power of the fundamental component.

- The signal to noise and distortion ratio (SINAD) is defined as the ratio of the total power of the signal to the combined power of noise and distortion.

➢ *Data distribution and autocorrelation features*

- The 'Distribution features section' contains conventional statistical characteristics that describe the overall distribution of the data. The features include the lowest value, the middle value, the highest value, quartile statistics and user-defined quantiles for a given value.
- The 'Autocorrelation features section' contains features that represent the linear relationship between a variable and itself at two different time points. For stationary processes, only the time lag between two locations determines the autocorrelation between them. The autocorrelation function is a sequence that represents the autocorrelation values for each potential lag value. The sum of squares for a given value of *n* is the sum of squares of the first *n* autocorrelations.
- The 'Partial autocorrelation features section' contains features that are comparable to the autocorrelation features. However, these features take into consideration the influence of mutual linear dependency on other variables in the sequence. The partial autocorrelation function (PACF) is a sequence that represents the partial autocorrelations for different lag values. The sum of squares for a given value of *n* is the sum of squares of the first *n* partial autocorrelations.

2) Frequency domain features

In this step, you must define the frequency range in which the spectral properties of the ECG signal are to be analyzed. Setting the lower and upper limits of this frequency range is crucial because it determines which parts of the signal's frequency spectrum are taken into account in the spectral analysis. By specifying these limits, you ensure that the analysis focuses on the relevant frequency components, which can improve the accuracy of feature extraction and subsequent modeling. This step is important to isolate specific frequency bands that are critical to recognizing and interpreting the underlying patterns in the ECG signal and ultimately contribute to the effective monitoring and prediction of electrolyte levels.

➢ *Spectral peaks*

By analyzing the amplitude of these peaks, one can create a feature. Calculate a feature by analyzing the frequency at which the peaks occur.

➢ *Peaks*

The quantity of peaks for which generated feature is created. Identify the most prominent peaks within the selected frequency range and arrange them in order of decreasing amplitude.

➢ *The minimum threshold for the peak value*

To exclude peaks with low amplitudes, limit the maximum size of the peaks to exclude those with low amplitudes.

➢ *Minimum frequency gap*

Specify the minimum difference in frequency. If the distance between two peaks is smaller than this specified value, the software disregards the smaller peak of the pair.

➢ *Peak excursion tolerance*

It refers to the minimum prominence required for a peak to be taken into account. The prominence of a peak quantifies its distinctiveness based on its inherent height and its position relative to neighboring summits.

3) Time-frequency domain features

Signals with non-stationary frequencies that shift over time are characterized by time-frequency features. These signals can originate from machinery that has deteriorated or experienced a hardware failure.

Frequency domain feature extraction commonly involves the use of power spectral density (PSD), spectral entropy, often referred to as SE and the sum SMNR. You can calculate the PSD using:

$$S(k) = \frac{1}{N}\left|\sum_{n=0}^{N-1} x(n)e^{-j2\pi fn}\right|^2 = \frac{1}{N}|X(k)|^2 \qquad (9)$$

This is the Fourier transform of the sample sequence *x(n)*, as cited in [31], [32]:

The SE is a measure of signal irregularity, which can be obtained by applying the Shannon entropy approach to the normalized signal power distribution as below [33]-[36]:

$$H = -\sum_{m=1}^{N} p(k)\log_2 p(k) \qquad (10)$$

where H is the SE, N is the total number of frequency points and $p(k)$ is the power distribution of the Fourier-transformed signal normalized to a power unit.

➢ *Spectrogram features*

Features derived from the examination of spectrograms. The following features are included:

The spectral kurtosis (SK) metric measures the presence of transients in a signal by assigning low values to frequencies consisting predominantly of stationary Gaussian noise and high values to frequencies with transients. We specify the window size as "10".

SE quantifies the fluctuations in the spectral power distribution of a signal over time. Significant fluctuations in value can indicate flaws.

➢ *Empirical mode decomposition features*

Characteristics derived from the empirical mode decomposition (EMD). The EMD of a signal quantifies the degree of randomness and unpredictability in the frequency content of the signal. An increase in the value may indicate the existence of a fault and the energy derived from the intrinsic mode function (IMF) signal generated by the EMD calculation. There are three IMFs.

The Hilbert-Huang transform (HHT) is useful for time-frequency analysis of non-stationary and non-linear data. The HHT is used to calculate the analytical signal [40]-[41].

The EMD method is an important part of the HHT and allows the decomposition of arbitrary data into a finite number of IMFs. Therefore, we can express signal $X(t)$ as follows:

$$X(t) = \sum_{i=1}^{n} imf_i(t) + r_n(t) \tag{11}$$

where *I = 1...*, *n* is the number of IMFs.

Wavelet entropy (*WE*) is a commonly used feature in various fields to quantify signal disorder. In the following expressions, the normalized power is denoted by the "*p*" value [38]-[39].

$$WE = -\sum_{m=1}^{N} p(k) \log_2 p(k) \tag{12}$$

This is the wavelet coefficient and the probability distribution of the wavelet energy.

Finally, we include the demographic information of the patients from whom we take blood samples. We represent these numerically using ICD codes and specific age groups. The final feature vector consists of a total of 61 elements.

D. Feature selection

Feature selection is a crucial step in ML, which is about determining the most relevant features for creating a model. The F-test is a method commonly used for feature selection. It has been the focus of numerous research efforts aimed at improving its use in diverse fields.

The optimization of F-measures in feature selection aims to reduce the imbalance between classes by assigning different costs to each class. This approach focuses on selecting features that accurately reflect all classes, not just the majority class. This improves the performance of models on imbalanced datasets [42].

In this study, 10 features that had the best F-value were selected. One of the most popular supervised feature selection methods is the Fisher score. However, it selects each feature separately based on how well it scores using the Fisher criterion, resulting in suboptimal selection of features. The ratio between the average intraclass separation and the average interclass separation is called the Fisher score. The feature's ability to discriminate increases with a higher Fisher score. It is calculated in this way:

$$F = \frac{\sum_{j=1}^{k} p_j(\mu_j - \mu)^2}{\sum_{j=1}^{k} p_j \sigma_j^2} \tag{13}$$

The following terms are defined:

- μ_j: The mean of the data points in a specific class for a particular feature.
- σ_j: The standard deviation of the data points in a specific class for a given feature.
- p_j: The fraction of data points belonging to a specific class.
- μ: The global average of the data pertaining to the attribute.

Use the above formula to determine which feature has a greater degree of discriminative power.

Table 4 and Table 5 show the feature importance scores for calcium and potassium, ranked using the F-test algorithm. Each row represents a different feature related to ECG measurements, with the corresponding F-test scores indicating the importance or significance of each feature in the context of the analysis.

Table 4. Feature importance scores ranked using the F-test algorithm for calcium.

ID	Feature	F-test
1	ECG - Peak amplitude 1	5.7865
2	ECG - EMD/energy – IMF2	4.5560
3	ECG - Crest factor	3.6895
4	ECG - Morphological/ QT interval	3.1012
5	ECG - RMS	3.0393
6	ECG - Standard deviation	2.7254
7	ECG - Autocorrelation value ACF1	2.4775
8	ECG - Partial autocorrelation value PACF1	2.4775
9	ECG - Impulse factor	2.4223
10	ECG - Minimum value	2.3894

Table 5. Feature importance scores ranked using the F-test algorithm for potassium.

ID	Feature	F-test
1	ECG - Spectrogram/peak value	5.3778
2	ECG - Spectrogram/clearance factor	3.8139
3	ECG - Partial autocorrelation value PACF5	3.7532
4	ECG - Morphological/ PR segment	3.5735
5	ECG - Peak amplitude 1	3.4404
6	ECG - Crest factor	2.7231
7	ECG - Autocorrelation value ACF10	2.4363
8	ECG - Impulse factor	2.4075
9	ECG - Autocorrelation value ACF1	2.0123
10	ECG - Partial autocorrelation value PACF1	2.0123

E. Regression methods

This section describes widely-used modeling approaches based on the regression-based FIS and NN regression (NN-R).

1) Neural network - regression

In this study, a multilayer feed-forward artificial NN was used. The investigations revealed a multi-layered structure with three intermediate layers. We decided that the dimensions of the layers should be at least half the number of input characteristics. We must ensure that the total number of

parameters computed in the hidden layer is less than the number of samples in the training set. Otherwise, the resulting NN structure will have perfect storage of all inputs, rendering learning impossible.

Feedforward-controlled ANNs are NNs that have an input layer, an output layer and one or more intermediate layers. These networks use different activation parameters to transfer information from the input layer to the output layer in one direction. Additionally, there is no connection between cells within the same layer. We can use different methods to determine the number of cells in the hidden layer. However, a process of trial and error typically establishes the cell count [43].

The hidden layer output vector $h = (h_1, h_2, h_s)$ is obtained from the network input vector $x = (x_1, x_2, x_k)$ and after being processed in the output layer converted into the output vector $y = (y_1, y_2, y_z)$, and output vectors *Y = [y(1), ..., y(N)]*, where *N* is the number of input and output vectors and is calculated for all considered input vectors *X = [x (1) ..., x(N)]* as follows:

$$Y = \varphi(W^y[\psi(W^h X + b^h)] + b^y) \tag{14}$$

where $\varphi(.)$ and $\psi(.)$ represent the activation functions of the cells in the output layer and the hidden layer, respectively. Both the hidden layer and the output layer provide the user with a boundary value vector for their cells. The numbers 10, 4, and 1 in Fig. 8 represent the sample size, number of layers, and number of output units, respectively.

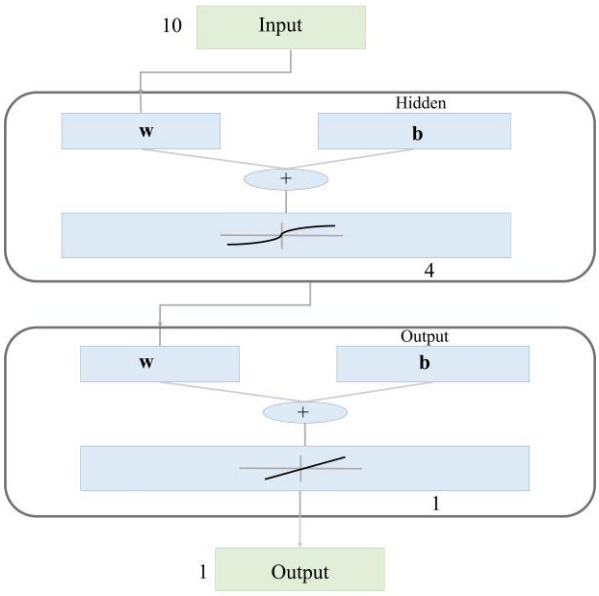

Fig. 8. Diagram of NN.

The model parameters chosen here for the NN-R model are as follows: a two-layer feedforward network with one hidden layer consisting of four neurons using a sigmoid activation function, an output layer with a single neuron using a linear activation function, and the Levenberg-Marquardt method as the training algorithm.

A two-layer feedforward network is an artificial NN model that enables the systematic transformation of inputs into outputs through unidirectional data flow. This network consists of a hidden layer with four layers, each using a sigmoid activation function, and an output layer consisting of a single neuron using a linear activation function. The sigmoid function in the hidden layer normalizes the inputs to a range between 0 and 1, which helps in learning non-linear characteristics. On the other hand, the linear function in the output layer provides direct results and is therefore suitable for regression analysis and applications that require continuous value predictions.

The Levenberg-Marquardt method is used as the training algorithm in this model. This approach is well-known for its efficiency in dealing with non-linear least squares problems that help to optimize the performance of the network.

2) Regression-based FIS

FIS are computational frameworks that integrate the advantages of fuzzy logic and inferential reasoning to effectively manage uncertainties and inaccuracies in data. They are especially valuable in situations where conventional binary logic systems are insufficient. This is a revolutionary type-2 FIS that does not impose explicit rules and can handle numerous variables. The system uses Gaussian membership functions to represent the inputs and uses linearly parameterized system functions to derive the output. A genetic algorithm is used to determine the system parameters based on a multi-objective function. This approach combines the evolutionary algorithm with a feature selection method and a regularized ridge regression. The goal of the functions consists of two components: the tally of active features and the validation error for regression models or the accuracy for classification models. The aim of this method is to achieve a harmonious balance between the quality of the model and its simplicity. The improved approach, using type-2 fuzzy sets, shows superior efficiency compared to previous systems based on type-1 fuzzy sets across a number of trials, including function approximation, fuel consumption prediction, breast tissue classification and concrete compressive strength prediction [44].

F. Performance metrics

Regression analysis is a critical component of supervised ML, which involves predicting a continuous target variable based on predictor factors. Individuals often evaluate the effectiveness of regression models using different criteria, although they cannot agree on a universally accepted criterion.

The metrics *R* and mean square error (*MSE*) provide more comprehensive and insightful information compared to other measures. The coefficient of determination, referred to as *R*, is considered superior to other metrics for evaluating regression analysis. This is because *R* only provides a high score when a large portion of the actual values are accurately

predicted, overcoming the limitations in interpretability that occur with other metrics [45].

$$MSE = \frac{1}{N}\sum_{i=1}^{N}(y_i - \hat{y})^2 \quad (15)$$

$$R = \sqrt{1 - \frac{\sum(y_i - \hat{y})^2}{\sum(y_i - \hat{y})^2}} \quad (16)$$

where y_i is the actual ion concentration value, the ion concentration estimate value. N represents the number of samples.

The study does not contain individual patient data or information. The study contains no identifiable or recognizable information. It is declared that there is no conflict of interest and that the privacy of the research participants will be respected. It is imperative that this research is not used directly in clinical care. Additional validation and testing using variance data sets are necessary to assess potential bias. The study accurately cites the material and research sources used. We have taken all necessary measures to ensure that the study is based on the most accurate and up-to-date information available. All relevant sources have been cited in accordance with the standards for academic integrity established by the organization.

5. RESULTS AND DISCUSSION

MIMIC III contains many clinical datasets in scattered form. Therefore, those datasets that meet the necessary conditions were filtered and matched with electrical signals such as the ECG. Attributes were forged by using different techniques on ECG signals resulting from these matches. Our aim was to compare the performance results, performance training and validation processes with the NN-R and regression-based FIS methods, accepted as part of the regression model.

Hold-out validation is a technique used to assess the predicted performance of statistical models. It involves splitting the data into separate sets for training and testing. For datasets with uneven class distribution, particularly with rare classes, repeated hold-out validation is recommended as the most appropriate validation approach [46].

Hold-out refers to the process of dividing a dataset into two different sets, namely the 'training' set and the 'test' set. The model is trained using the training set and its performance is evaluated on new data using the test set. An often-used division when applying the hold-out method is to use 70 % of the data for training purposes and reserve the remaining 30 % for testing.

Morphological, frequency and time-frequency domain-based attribute data from patients were used as input to the regression model to estimate the blood calcium and potassium values of patients. The performance results of NN-R and FIS are shown in Table 6 and Table 7.

Table 6. Regression results for potassium.

Dataset type	Regression methods	*MSE*	*R*
Train set	NN-R	0.1753	0.85636
	Regression-based FIS	0.5235	0.45189
Validation set	NN-R	2.2248	0.24328
	Regression-based FIS	0.3162	0.60699

Table 7. Regression results for calcium.

Dataset type	Regression methods	*MSE*	*R*
Train set	NN-R	0.3674	0.53613
	Regression-based FIS	0.4142	0.4531
Validation set	NN-R	1.1698	0.061436
	Regression-based FIS	0.7157	0.57347

This study focuses on the calculation of potassium and calcium levels in patients with CKD using ECG measurements. There are 116 recorded cases of potassium and 101 recorded cases of calcium, respectively. The observations were randomly split into two groups:

- a training group, which comprised 70 % of the data, and
- a validation group, which comprised 30 % of the data.

The training set, known as the potassium dataset, consists of 84 records, while the validation set contains 32 records. The calcium dataset consists of 81 records for training and 30 records for validation. The components of the input vector x can be found in Table 1. The variable y reflects the combined value of potassium and calcium. The ridge regression value is set to $R = 1x10^6$ for the training set and $R = 1x10^9$ for the validation set of the potassium dataset. For the calcium dataset, the regularization parameter is $R = 0.4531$ for the training set and $R = 0.57347$ for the validation set. The population size for the multi-objective genetic algorithm is determined by the number of variables in each individual, denoted as *n*. The number of iterations is 50, resulting in 50 assessments of the objective function. The models under consideration generate the actual value of *y*.

Fig. 9, labeled *"Calcium training: R = 0.4531"*, shows a scatter plot illustrating the correlation between the desired calcium values and the actual calcium values recorded during the training period. The graph also contains a linear regression line. The *R*-value of 0.4531 indicates a somewhat positive correlation between the targets and outputs, which means that the model's predictions are somewhat aligned with the actual values, but not perfectly. The regression equation *"Calcium value = 0.275 × Target + 6.3"* in the first graph shows that the measured output values do not perfectly align with the target values.

Fig. 10 is labeled *"Calcium validation: R = 0.57347"* and shows a model validation setup with a linear regression line. The increased *R*-value in the validation phase compared to the training phase indicates a small improvement in the correlation. The regression equation *"Calcium*

value = 0.93 × Target + 5" from the second graph shows that for every increase in the calcium target value by one unit, the calcium value output increases by 0.93 units.

Both plots feature a dotted line labeled *"Y = T"*, which shows the optimal scenario where the measured values perfectly align with the target values. Nevertheless, the scattering of data points from the ideal line in both graphs indicates that the model does not fully reflect the correlation between the desired and observed values.

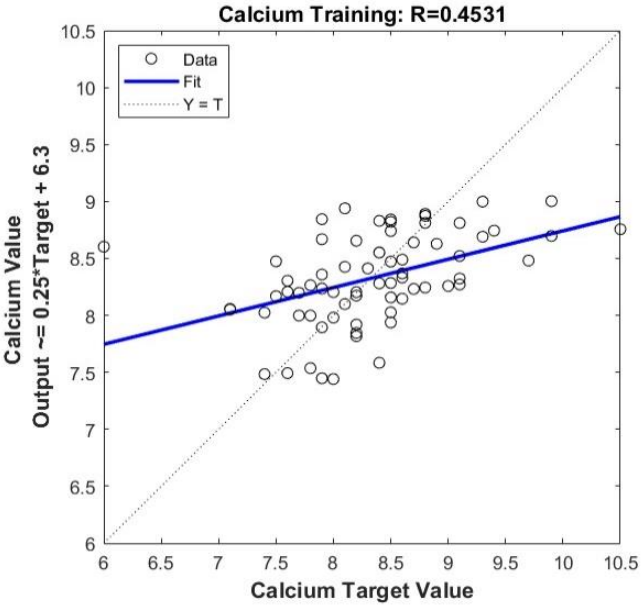

Fig. 9. FIS-Regression graph of training for calcium.

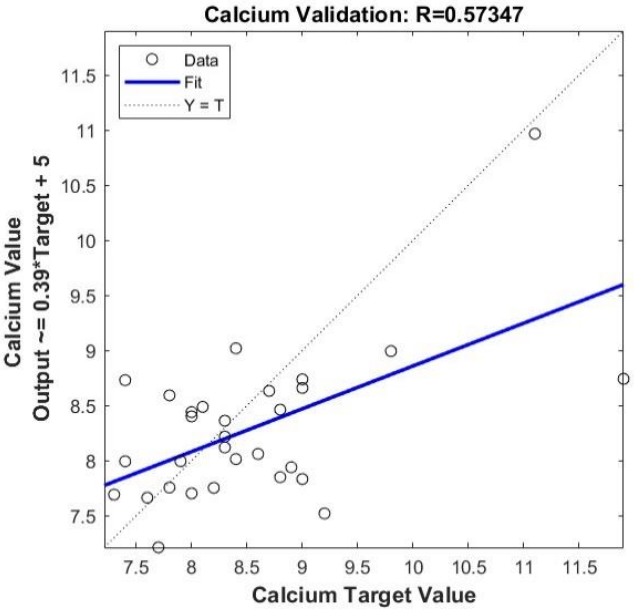

Fig. 10. FIS-Regression graph of validation for calcium.

Fig. 11 and Fig. 12 show the training and validation phases of a model based on potassium data. The graph labeled *"Potassium training: R = 0.45189"* shows the data used for training and the corresponding linear regression fit. The next graph, labeled *"Potassium validation: R = 0.60699"* shows the validation data and the regression fit.

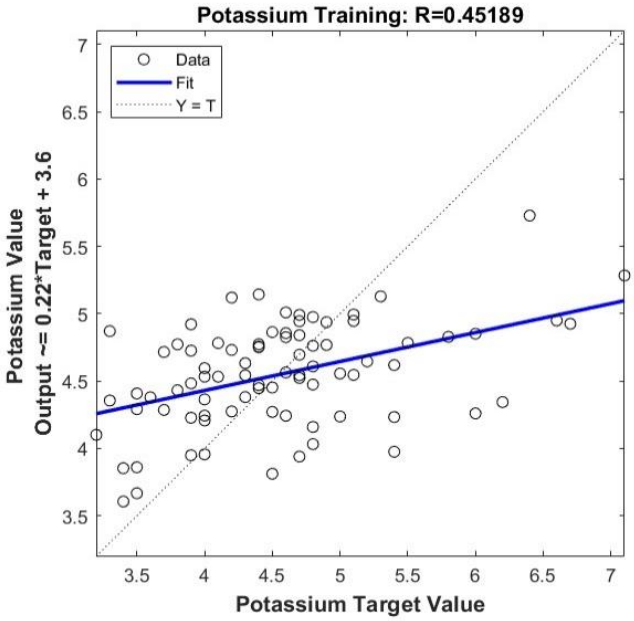

Fig. 11. FIS-Regression graph of training for potassium.

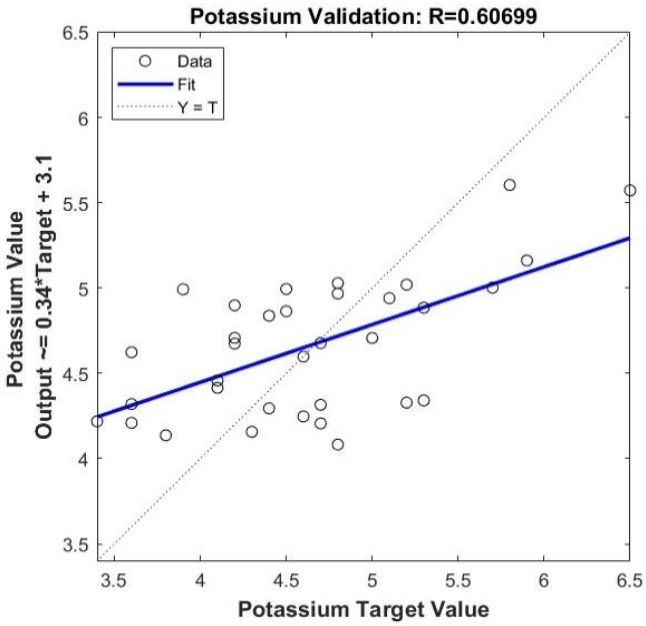

Fig. 12. FIS-Regression graph of validation for potassium.

This NN architecture with the sigmoid activation function in the hidden layer for non-linear capabilities and the linear activation function in the output layer for direct output allows modeling of complicated interactions and can be used with diverse datasets. The backpropagation algorithm, which iteratively modifies the network's weights to minimize the error rate in the dataset, performs the network's training phase. A loss function commonly quantifies this process by assessing and optimizing the degree of agreement between

the model's predictions and the real values. In this step, you need to define the lower and upper frequency limits for the range used to calculate the spectral characteristics of the data. This is crucial for optimizing the performance of the Levenberg-Marquardt training algorithm, which is used to minimize the *MSE* during model training. By selecting an appropriate frequency range, you ensure that the extracted spectral features are relevant and contribute to improving the accuracy of the model. This process helps to fine-tune the algorithm's performance and results in a more effective and reliable predictive model.

During the training process of a two-layer feedforward network with the Levenberg-Marquardt algorithm, the model improves significantly, as shown by the metrics that are tracked across epochs. From epoch 0 to 1000, there is a significant improvement in performance as shown by the decrease in mean square error from 1.13 to 0.151. This decrease indicates an improved prediction accuracy. At the same time, the gradient decreases from 1.82 to 0.00156, indicating successful error reduction, while the damping factor *Mu* adjusts from 0.001 to $1x10^6$, optimizing the trade-off between gradient descent and least squares fit. The validation tests remain consistently at 0 throughout, indicating that the model is continuously improving without overfitting. This demonstrates the efficiency of the Levenberg-Marquardt algorithm in improving the accuracy and reliability of the network over time.

The following three graphs evaluate a NN-R model's ability to predict calcium levels.

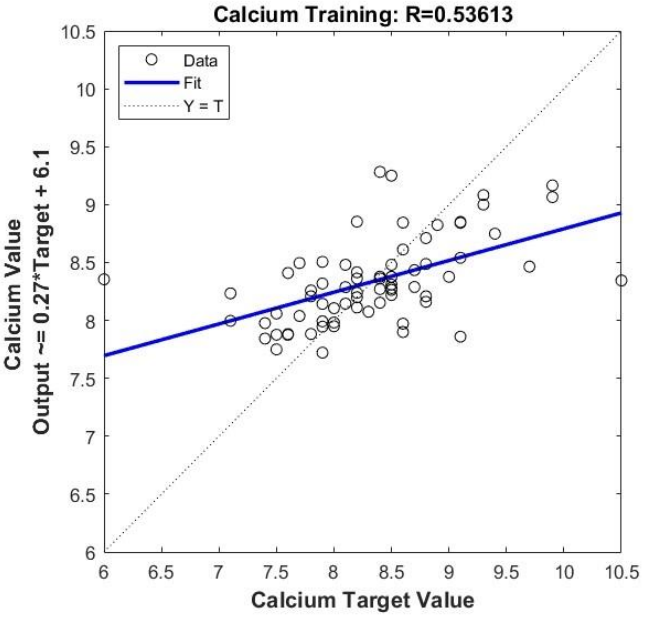

Fig. 13. NN-R graph of training for calcium.

Fig. 13 and Fig. 14 show the recorded output values compared to the target calcium values for both the training and validation stages of the model. The training graph shows a correlation coefficient $R = 0.53613$ indicating a moderate positive correlation between the targets and outputs. This indicates that the data fits the linear regression line reasonably well. The validation graph shows an unexpectedly low *R*-value of 0.061436, indicating a weak correlation between target and output. This could indicate that the validation data differs significantly from the training data or that the model has been over-fitted to the training data and is unable to generalize effectively.

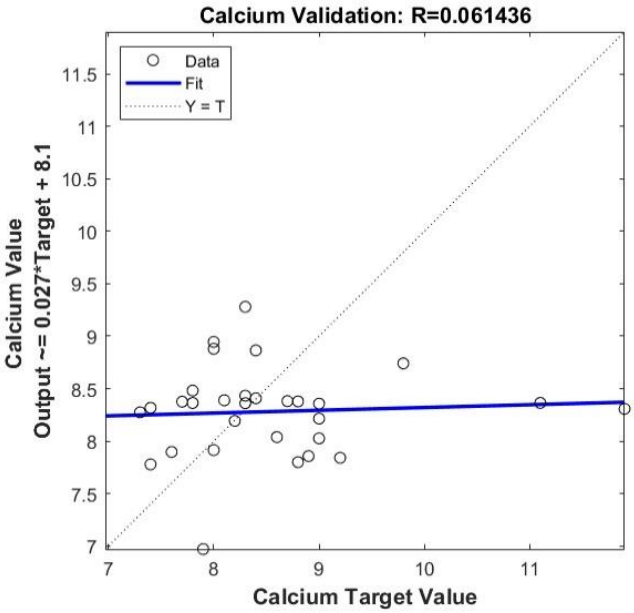

Fig. 14. NN-R graph of validation for calcium.

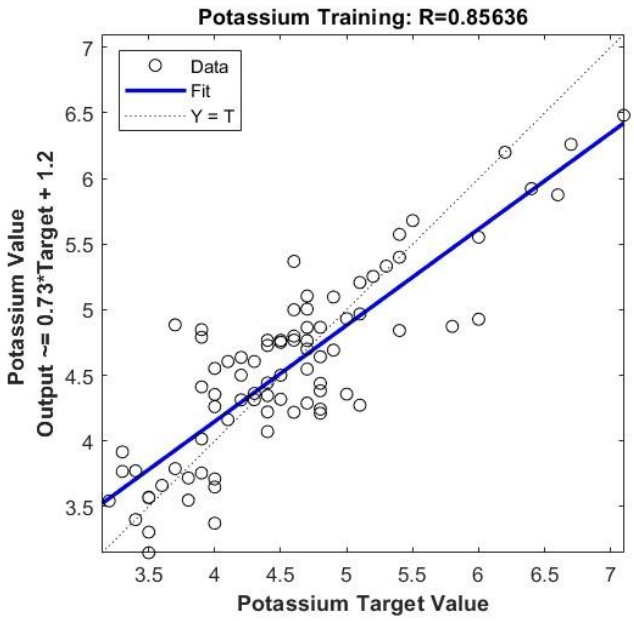

Fig. 15. NN-R graph of training for potassium.

Fig. 15 and Fig. 16, *"Potassium training: R = 0.85636"*, show a strong positive correlation between the target and measured potassium values during the training phase. *"Potassium validation: R = 0.24328"* also shows the

validation phase data with a significantly lower R value. This indicates a weaker correlation and suggests that the model does not generalize well to new data on which it has not been trained.

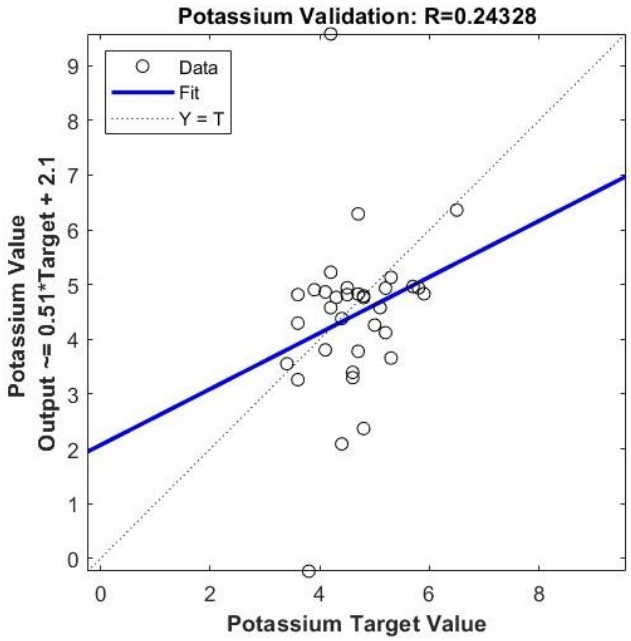

Fig. 16. NN-R graph of validation for potassium.

Summarizing the dataset for the prediction of potassium and calcium models shows different performances between the different regression methods and types of datasets. The NN-R for potassium shows remarkable performance in the training set, with a substantial *R*-value of 0.85636 and a minimum *MSE* of 0.1753. These values indicate robust prediction accuracy. However, the model's performance significantly decreases in the validation set, as indicated by a substantial *MSE* of 2.2248 and a low correlation coefficient *R*-value of 0.24328, which indicates overfitting. On the other hand, the regression-based FIS shows a higher consistency in its performance. It achieves moderate *R*-values of 0.45189 and 0.60699 and *MSE*s of 0.5235 and 0.3162 for the training and validation sets, respectively.

The NN-R for the calcium dataset shows a decline in performance when comparing the training set to the validation set. The *MSE* decreases from 0.3674 to 1.1698, while the *R*-value decreases from 0.53613 to 0.061436. In the training phase, the regression-based FIS shows a more consistent performance compared to the NN, even though it has a larger *MSE*. The *R*-value shows less variation, indicating better generalization from training to validation.

In general, while NN-Regression can accurately capture the patterns in the training data, as shown by the high *R*-values, it does not properly apply these patterns to new, unseen data. This leads to a significant decrease in performance when evaluating the model in the validation set. While the regression-based FIS is less accurate in the training set, it provides more consistent and reliable predictions for the unseen data.

6. CONCLUSION

The main objective of this work was to develop an automated method for predicting blood calcium and potassium levels from patients' ECG recordings. To do this, ECG signals were collected in conjunction with blood samples to create models capable of calculating the levels of these electrolytes. This innovative method has the potential to streamline the monitoring of key blood parameters and provide a non-intrusive and potentially immediate substitute for conventional blood testing.

The initial models in the study, using NN-R and regression-based FIS, had different levels of success. While the NNs performed remarkably well on the training data, they could not maintain accuracy on the validation sets. This difference highlights the need to improve the models to improve their ability to make accurate predictions in a wide range of situations. Furthermore, the large amount of features extracted from the ECG signals used as inputs for the model demonstrates the need for improvements. Further research will prioritize feature selection to optimize the model, increase computational efficiency, and potentially improve performance by reducing redundancy and emphasizing the most informative features.

Another important area for future improvement is to address the impact of outliers on model accuracy. Outliers can result from anomalies in the ECG readings or patient-specific factors and affect prediction accuracy. To ensure the practicality of the models, efforts to minimize these effects will be a key focus.

Existing research has primarily focused on the use of conventional blood tests to diagnose electrolyte imbalances and on further development of non-invasive methods that use bio-signals such as the ECG to estimate electrolyte concentrations. Several studies have investigated the extraction of morphological, frequency and time-frequency features from ECG signals. These studies have used ML models to estimate potassium and calcium levels. Nevertheless, most of these technologies have not been well evaluated in terms of accuracy and robustness, nor do they provide a thorough investigation of the practicality and effectiveness of using non-invasive techniques for continuous monitoring.

This study stands out from others by exploring the application of machine learning and ECG recordings in monitoring potassium and calcium levels, as well as conducting a comprehensive analysis of the potential of FIS to improve estimation accuracy. Our approach combines FIS with feature extraction from ECG signals to predict electrolyte concentrations, particularly calcium. This integration has led to encouraging results in terms of *MSE* and correlation coefficient *R*. This study contributes to the field

by demonstrating that FIS can provide a clearer and more efficient model for continuous and non-invasive monitoring of essential electrolyte levels. This addresses the shortcomings of current methods and supports the development of diagnostic tools that can be used at home.

In the future, other physiological signals such as photoplethysmography (PPG) and the measurement of arterial blood pressure (ABP) will also be included in the study. By integrating these data, we can improve the accuracy and reliability of the models, leading to a comprehensive understanding of the patient's cardiovascular condition and its relationship to blood electrolyte levels.

In essence, this research represents a significant milestone in the advancement of automated, non-invasive diagnostic methods. The results of this study have the potential to completely transform the management and monitoring of patients, particularly those who require frequent electrolyte level monitoring. Future studies will improve and extend the approaches used by incorporating a wider range of signals. This will lead to the development of more advanced and reliable prediction models that will ultimately improve patient care and healthcare outcomes.

REFERENCES

[1] Hill, N. R., Fatoba, S. T., Oke, J. L., Hirst, J. A., O'Callaghan, C. A., Lasserson, D. S., Hobbs, F. D. R. (2016). Global prevalence of chronic kidney disease – a systematic review and meta-analysis. *PLoS One*, 11 (7), e0158765. https://doi.org/10.1371/journal.pone.0158765

[2] Coresh, J., Selvin, E., Stevens, L. A., Manzi, J., Kusek, J. W., Eggers, P., Van Lente, F., Levey, A. S. (2007). Prevalence of chronic kidney disease in the United States. *Jama*, 298 (17), 2038-2047. https://doi.org/10.1001/jama.298.17.2038

[3] Sarnak, M. J., Levey, A. S., Schoolwerth, A. C., Coresh, J., Culleton, B., Hamm, L. L., McCullough, P. A., Kasiske, B. L., Kelepouris, E., Klag, M. J., Parfrey, P., Pfeffer, M., Raij, L., Spinosa, D. J., Wilson, P. W. (2003). Kidney disease as a risk factor for development of cardiovascular disease: A statement from the American Heart Association Councils on Kidney in Cardiovascular Disease, High Blood Pressure Research, Clinical Cardiology, and Epidemiology and Prevention. *Circulation*, 108 (17), 2154-2169. https://doi.org/10.1161/01.CIR.0000095676.90936.80

[4] Lin, C.-S., Lin, C., Fang, W.-H., Hsu, C.-J., Chen, S.-J., Huang, K.-H., Lin, W.-S., Tsai, C.-S., Kuo, C.-C., Chau, T., Yang, S. J. H., Lin, S.-H. (2020). A deep-learning algorithm (ECG12Net) for detecting hypokalemia and hyperkalemia by electrocardiography: Algorithm development. *JMIR Medical Informatics*, 8 (3), e15931. https://doi.org/10.2196/15931

[5] Priori, S. G., Blomström-Lundqvist, C., Mazzanti, A., Blom, N., Borggrefe, M., Camm, J., Elliott, P. M., Fitzsimons, D., Hatala, R., Hindricks, G., Kirchhof, P., Kjeldsen, K., Kuck, K. H., Hernandez-Madrid, A., Nikolaou, N., Norekvål, T. M., Spaulding, C., Van Veldhuisen, D. J., ESC Scientific Document Group. (2015). 2015 ESC Guidelines for the management of patients with ventricular arrhythmias and the prevention of sudden cardiac death: The Task Force for the Management of Patients with Ventricular Arrhythmias and the Prevention of Sudden Cardiac Death of the European Society of Cardiology (ESC). Endorsed by: Association for European Paediatric and Congenital Cardiology (AEPC). *European Heart Journal*, 36 (41), 2793-2867. https://doi.org/10.1093/eurheartj/ehv316

[6] McIntosh, B. W., Vasek, J., Taylor, M., Le Blanc, D., Thode, H. C., Singer, A. J. (2018). Accuracy of bedside point of care testing in critical emergency department patients. *American Journal of Emergency Medicine*, 36 (4), 567-570. https://doi.org/10.1016/j.ajem.2017.09.018

[7] Gavala, A., Myrianthefs, P. (2017). Comparison of point-of-care versus central laboratory measurement of hematocrit, hemoglobin, and electrolyte concentrations. *Heart & Lung*, 46 (4), 246-250. https://doi.org/10.1016/j.hrtlng.2017.04.003

[8] Dylewski, J. F., Linas, S. (2018). Variability of potassium blood testing: Imprecise nature of blood testing or normal physiologic changes? *Mayo Clinic Proceedings*, 93 (5), 551-554. https://doi.org/10.1016/j.mayocp.2018.03.019

[9] Diercks, D. B., Shumaik, G. M., Harrigan, R. A., Brady, W. J., Chan, T. C. (2004). Electrocardiographic manifestations: Electrolyte abnormalities. *The Journal of Emergency Medicine*, 27 (2), 153-160. https://doi.org/10.1016/j.jemermed.2004.04.006

[10] Slovis, C., Jenkins, R. (2002). ABC of clinical electrocardiography: Conditions not primarily affecting the heart. *BMJ*, 324 (7349), 1320-1323. https://doi.org/10.1136/bmj.324.7349.1320

[11] Van Mieghem, C., Sabbe, M., Knockaert, D. (2004). The clinical value of the ECG in noncardiac conditions. *Chest*, 125 (4), 1561-1576. https://doi.org/10.1378/chest.125.4.1561

[12] Periz, L. A., Sanmartín, E. F. (2001). *500 Cuestiones QUE Plantea El Cuidado Del Enfermo Renal (2ª Ed.)*. Elsevier España, p. 410. ISBN 9788445810828.

[13] Halperin, M. L., Kamel, K. S. (1998). Potassium. *The Lancet*, 352 (9122), 135-140. https://doi.org/10.1016/S0140-6736(98)85044-7

[14] Szerlip, H. M., Weiss, J., Singer, I. (1986). Profound hyperkalemia without electrocardiographic manifestations. *American Journal of Kidney Diseases*, 7 (6), 461-465. https://doi.org/10.1016/S0272-6386(86)80185-8

[15] Schaefer, T. J. Wolford, R. W. (2005). Disorders of potassium. *Emergency Medicine Clinics*, 23 (3), 723-747. https://doi.org/10.1016/j.emc.2005.03.016

[16] Webster, A., Brady, W., Morris, F. (2002). Recognising signs of danger: ECG changes resulting from an abnormal serum potassium concentration. *Emergency Medicine Journal*, 19 (1), 74-77. https://doi.org/10.1136/emj.19.1.74

[17] Evans, K. J., Greenberg, A. (2005). Hyperkalemia: A review. *Journal of Intensive Care Medicine*, 20 (5), 272-290. https://doi.org/10.1177/0885066605278969

[18] Fisch, C. (1973). Relation of electrolyte disturbances to cardiac arrhythmias. *Circulation*, 47 (2), 408-419. https://doi.org/10.1161/01.CIR.47.2.408

[19] Frohnert, P. P., Giuliani, E. R., Friedberg, M., Johnson, W. J., Tauxe, W. N. (1970). Statistical investigation of correlations between serum potassium levels and electrocardiographic findings in patients on intermittent haemodialysis therapy. *Circulation*, 41 (4), 667-676. https://doi.org/10.1161/01.CIR.41.4.667

[20] Corsi, C., De Bie, J., Napolitano, C., Priori, S., Mortara, D., Severi, S. (2012). Validation of a novel method for non-invasive blood potassium quantification from the ECG. In *2012 Computing in Cardiology*. IEEE, 105-108. https://ieeexplore.ieee.org/document/6420341

[21] Corsi, C., Cortesi, M., Callisesi, G., De Bie, J., Napolitano, C., Santoro, A., Mortara, D., Severi, S. (2017). Noninvasive quantification of blood potassium concentration from ECG in hemodialysis patients. *Scientific Reports*, 7 (1), 42492. https://doi.org/10.1038/srep42492

[22] Mesa, M. H., Pilia, N., Dössel, O., Loewe, A. (2019). Influence of ECG lead reduction techniques for extracellular potassium and calcium concentration estimation. *Current Directions in Biomedical Engineering*, 5 (1), 69-72. https://doi.org/10.1515/cdbme-2019-0018

[23] Sánchez, J. L. C., Camarero, A. R. A., Pérez, M. C., Sota, M. M. Á., Llamazares, C. V., Roldán, C. H., Viadero, R. M., Nates, R. A. (2012). Hyperkalaemia and haemodialysis patients: Electrocardiographic changes. *Journal of Renal Care*, 33 (3), 124-129. https://doi.org/10.1111/j.1755-6686.2007.tb00057.x

[24] Mesa, M. H., Pilia, N., Dössel, O., Severi, S., Loewe, A. (2018). Effects of serum calcium changes on the cardiac action potential and the ECG in a computational model. *Current Directions in Biomedical Engineering*, 4 (1), 251-254. https://doi.org/10.1515/cdbme-2018-0061

[25] Pilia, N., Dössel, O., Lenis, G., Loewe, A. (2017). ECG as a tool to estimate potassium and calcium concentrations in the extracellular space. In *2017 Computing in Cardiology (CinC)*. IEEE. https://doi.org/10.22489/CinC.2017.265-080

[26] Dillon, J. J., DeSimone, C. V., Sapir, Y., Somers, V. K., Dugan, J. L., Bruce, C. J., Ackerman, M. J., Asirvatham, S. J., Striemer, B. L., Bukartyk, J., Scott, C. G., Bennet, K. E., Mikell, S. B., Ladewig, D. J., Gilles, E. J., Geva, A., Sadot, D., Friedman, P. A. (2015). Noninvasive potassium determination using a mathematically processed ECG: Proof of concept for a novel "blood-less, blood test". *Journal of Electrocardiology*, 48 (1), 12-18. https://doi.org/10.1016/j.jelectrocard.2014.10.002

[27] Johnson, A. E. W., Pollard, T. J., Shen, L., Lehman, L. H., Feng, M., Ghassemi, M., Moody, B., Szolovits, P., Celi, L. A., Mark, R. G. (2016). MIMIC-III, a freely accessible critical care database. *Scientific Data*, 3, 160035. https://doi.org/10.1038/sdata.2016.35

[28] Pilia, N., Nagel, C., Lenis, G., Becker, S., Dössel, O., Loewe A. (2021). ECGdeli - An open source ECG delineation toolbox for MATLAB. *SoftwareX*, 13, 100639. https://doi.org/10.1016/j.softx.2020.100639

[29] Metze, F., Ajmera, J., Englert, R., Bub, U., Burkhardt, F., Stegmann, J., Muller, C., Huber, R., Andrassy, B., Bauer, J. G., Little, B. (2007). Comparison of four approaches to age and gender recognition for telephone applications. In *2007 IEEE International Conference on Acoustics, Speech and Signal Processing - ICASSP '07*. IEEE. https://doi.org/10.1109/ICASSP.2007.367263

[30] Bocklet, T., Maier, A., Bauer, J. G., Burkhardt, F., Noth, E. (2008). Age and gender recognition for telephone applications based on GMM supervectors and support vector machines. In *2008 IEEE International Conference on Acoustics, Speech and Signal Processing*. IEEE, 1605-1608. https://doi.org/10.1109/ICASSP.2008.4517932

[31] Dempster, J. (2001). *The Laboratory Computer: A Practical Guide for Physiologists and Neuroscientists*. Academic Press, ISBN 978-0-12-209551-1. https://doi.org/10.1016/B978-0-12-209551-1.X5031-4

[32] Grami, A. (2015). Signals, systems, and spectral analysis. In *Introduction to Digital Communications*. Academic Press, 41-150. https://doi.org/10.1016/B978-0-12-407682-2.00003-X

[33] Pan, Y. N., Chen, J., Li, X. L. (2009). Spectral entropy: A complementary index for rolling element bearing performance degradation assessment. *Proceedings of the Institution of Mechanical Engineers, Part C: Journal of Mechanical Engineering Science*, 223 (5), 1223-1231. https://doi.org/10.1243/09544062JMES1224

[34] Sharma, V., Parey, A. (2016). A review of gear fault diagnosis using various condition indicators. *Procedia Engineering*, 144, 253-263. https://doi.org/10.1016/j.proeng.2016.05.131

[35] Shen, J.-L., Hung, J.-W., Lee, L.-S. (1998). Robust entropy-based endpoint detection for speech recognition in noisy environments. In *5th International Conference on Spoken Language Processing (ICSLP 1998)*. Rundle Mall, South Australia: Causal Production, 232-235. ISBN 1876346175.

[36] Vakkuri, A., Yli-Hankala, A., Talja, P., Mustola, S., Tolvanen-Laakso, H., Sampson, T., Viertiö-Oja, H. (2004). Time-frequency balanced spectral entropy as a measure of anesthetic drug effect in central nervous system during sevoflurane, propofol, and thiopental anesthesia. *Acta Anaesthesiologica Scandinavica*, 48 (2), 145-153. https://doi.org/10.1111/j.0001-5172.2004.00323.x

[37] Moghaddamnia, S., Peissig, J., Schmitz, G., Effenberg, A. O. (2013). A simplified approach for autonomous quality assessment of cyclic movements. In *2013 18th International Conference on Digital Signal Processing (DSP)*. IEEE. https://doi.org/10.1109/ICDSP.2013.6622672

[38] Coifman R. R., Wickerhauser, M. V. (1992). Entropy-based algorithms for best basis selection. *IEEE Transactions on Information Theory*, 38 (2), 713-718. https://doi.org/10.1109/18.119732

[39] Donoho, D. L., Johnstone, I. M. (1994). Ideal denoising in an orthonormal basis chosen from a library of bases. *Comptes Rendus de l'Académie des Sciences - Series I - Mathematics*, 319 (1), 1317-1322. https://imjohnstone.su.domains/WEBLIST/1994/idealbasis.pdf

[40] Huang, N. E., Shen, S. S. P. (Eds.) (2014). *Hilbert–Huang Transform and Its Applications (2nd Ed)*. World Scientific Publishing, Interdisciplinary Mathematical Sciences vol. 16, ISBN 9789814508230. https://doi.org/10.1142/8804

[41] Huang, N. E., Wu, Z., Long, S. R., Arnold, K. C., Chen, X., Blank, K. (2009). On instantaneous frequency. *Advances in Adaptive Data Analysis*, 1 (2), 177-229. https://doi.org/10.1142/S1793536909000096

[42] Liu, M., Xu, C., Luo, Y., Xu, C., Wen, Y., Tao, D. (2018). Cost-sensitive feature selection by optimizing F-measures. *IEEE Transactions on Image Processing*, 27 (3), 1323-1335. https://doi.org/10.1109/TIP.2017.2781298

[43] Walczak, S., Cerpa, N. (1999). Heuristic principles for the design of artificial neural networks. *Information and Software Technology*, 41 (2), 107-117. https://doi.org/10.1016/S0950-5849(98)00116-5

[44] Wiktorowicz, K. (2023). T2RFIS: Type-2 regression-based fuzzy inference system. *Neural Computing and Applications*, 35 (27), 20299-20317. https://doi.org/10.1007/s00521-023-08811-7

[45] Chicco, D., Warrens, M. J., Jurman, G. (2021). The coefficient of determination R-squared is more informative than SMAPE, MAE, MAPE, MSE and RMSE in regression analysis evaluation. *PeerJ Computer Science*, 7, e623. https://doi.org/10.7717/peerj-cs.623

[46] Silva, E., Zanchettin, C. (2016). On validation setup for multiclass imbalanced data sets. In *2016 5th Brazilian Conference on Intelligent Systems (BRACIS)*. IEEE, 468-473. https://doi.org/10.1109/BRACIS.2016.090

Received April 29, 2024
Accepted August 27, 2024